CrystEngComm

Accepted Manuscript

ROYAL SOCIETY OF CHEMISTRY

www.rsc.org/crystengcomm

CrystEngComm

COMMUNICATION

A Solvothermal Transformation from α-Fe$_2$O$_3$ Nanocrystals to Fe$_3$O$_4$ Polyhedrons

Liqiao Chen,[a,b]* Qingfeng Xiong,[c] Wenlin Li,[c] Junpeng Li,[c] and Xuan Yu[a]

High-dispersed Fe$_3$O$_4$ polyhedrons have been fabricated through a solvothermal transformation of α-Fe$_2$O$_3$ nanocrystals. The shapes, sizes, and surface characteristics of Fe$_3$O$_4$ polyhedrons can be facilely controlled. The growth route is confirmed as the process of " dissolution-reduction-recrystallization ". The saturation magnetization of as-prepared Fe$_3$O$_4$ is up to 102.2 emu/g.

Magnetite (Fe$_3$O$_4$) is attracting growing interest due to its great potential for many useful applications, such as magnetic fluids[1] and microwave absorption,[2] magnetic resonance imaging (MRI),[3, 4] drug delivery,[3, 5] catalytic and lithium storage properties.[6, 7] In recent years, micro- and nanoparticles for Fe$_3$O$_4$ with specific facets attracted considerable attention due to their abundant size- and shape-dependent physical and chemical properties.[8, 9] In addition, surface characteristics of Fe$_3$O$_4$ strongly affect its properties and applications.[10, 11]

As we know, fabrications of monodisperse Fe$_3$O$_4$ particles are often difficult due to its strong magnetism, especially for micrometer size Fe$_3$O$_4$ crystals, the as-obtained products are often with aggregation and wide size distribution even in the present of surfactants or complexing agents.[12, 13] In order to obtain high quality Fe$_3$O$_4$ crystals and prevent the aggregation of particles,[13] metal–organic iron precursor such as Fe (acac)$_3$ or Fe (CO)$_5$ are usually used, and / or designed the reaction in an organic medium, such as EG, oleic acid,[6, 8, 10, 14] which increase the costs and bring off environmental issue, also render the surface of as-obtained samples be dirty. The dirty surfaces affect its properties and bring some difficulty for

subsequent remove or surface modification.[15]

In addition, from a phase transformation viewpoint, Fe$_3$O$_4$ also can be obtained by reducing of Fe$_2$O$_3$ or oxidizing of Fe elemental. Fe$_3$O$_4$ nanoparticles are also synthesized by reduction phase transformation from γ-Fe$_2$O$_3$ nanoparticles in organic solvent.[16] microsized Fe$_3$O$_4$ with peanutlike morphology is successfully prepared from FeCO$_3$ with the same morphology via direct-sealed thermal decomposition.[17] Zhang etc. researched structural evolution and characteristics of the phase transformations between α-Fe$_2$O$_3$, Fe$_3$O$_4$ and γ-Fe$_2$O$_3$ nanoparticles under reducing and oxidizing atmospheres.[18] All the processes adopted a solid phase reaction under high-temperature, and many defects and impurities inevitably existed in the as-obtained crystals through these routes.

Herein, we find a novel solvothermal route to synthesize Fe$_3$O$_4$ polyhedrons through adopting only two reagents (See ESI†). That is α-Fe$_2$O$_3$ nanocrystals[19] can transform into Fe$_3$O$_4$ only in present of N$_2$H$_4$·H$_2$O (See ESI†), and no any other agent, surfactant and additive is brought. The detail condition is listed as table 1.

Table 1. The experimental condition synthesized Fe$_3$O$_4$ polyhedrons

	Precursor	N$_2$H$_4$·H$_2$O	Water	Temperature
Sample 1#	α-Fe$_2$O$_3$ nanoparticles	4 mL	2 mL	220 ℃
Sample 2#	α-Fe$_2$O$_3$ nanoplates	4 mL	2 mL	220 ℃
Sample 3#	α-Fe$_2$O$_3$ nanoparticles	4 mL	2 mL	180 ℃
Sample 4#	α-Fe$_2$O$_3$ nanoparticles	4 mL	no	220 ℃
Sample 5#	α-Fe$_2$O$_3$ nanoparticles	4 mL	4 mL	220 ℃

The powder X-ray diffraction patterns (pXRD) of as-synthesized Sample 1# in Figure 1a match well with JCPDS card No. 89-3854 for cubic Fe$_3$O$_4$ with a = b = c = 8.395 nm, confirming that all of products are cubic-structure iron oxide. However, it is difficult to distinguish the γ-Fe$_2$O$_3$ and Fe$_3$O$_4$ phases only from the XRD patterns due to their similarity. X-ray photoelectron spectroscopy

a. *Innovation & Application Institute, Zhejiang Ocean University, Zhoushan 316022, P. R. China. E-mail:chenlq118@126.com; Tel: +86 580 2262589.*
b. *State Key Laboratory of Optoelectronic Materials and Technologies, School of Chemistry and Chemical Engineering, Sun Yat-Sen University, Guangzhou 510275, P. R. China.*
c. *State Key Laboratory of Advanced Technologies for Comprehensive Utilization of Platinum Metals, Kunming Institute of Precious Metal, Kunming 650106, P. R. China.*

COMMUNICATION

CrystEngComm

(XPS) analysis (Figure 1b) was carried out to further ascertain the phase of the synthesized typical sample 1#. The binding energies relating to Fe $2p_{3/2}$ and Fe $2p_{1/2}$ are about 710.8, 725.2 eV, respectively, no satellite peak between the peaks of Fe $2p_{3/2}$ and Fe $2p_{1/2}$ are observed, indicating that the as-synthesized sample is composed of Fe_3O_4, which are in good agreement with those of Fe_3O_4 reported in the literature.[20] Therefore, XPS results also confirm the structure and phase of as-synthesized Fe_3O_4 products. The atom ratio of the product is determined as Fe (35.51%), O (64.49%) using XPS analysis. The oxygen content is higher than that of both Fe_3O_4, and α-Fe_2O_3. On one hand, it is probably because oxygen atoms are as the terminal atom layer for iron oxide crystals, which results in a higher oxygen detecting value near to the crystals' surfaces, on the other hand, it is also because the clean surfaces easily adsorb oxygen in the air. From the SEM image in Figure 1c, we can see that the product consists of highly dispersed decahedral microcrystals and the sizes of crystals are about 5 μm with narrow size distribution. The selected area electron diffraction (SAED) pattern, High-resolution transmission electron microscopy (HRTEM) and corresponding fast Fourier transformation (FFT) image verify that the as synthesized sample is cubic phase of structure, and the regular SAED patterns and clear Lattice fringes show the as-obtained powders are with high crystallinity (Figure 1d, 1e, 1f).
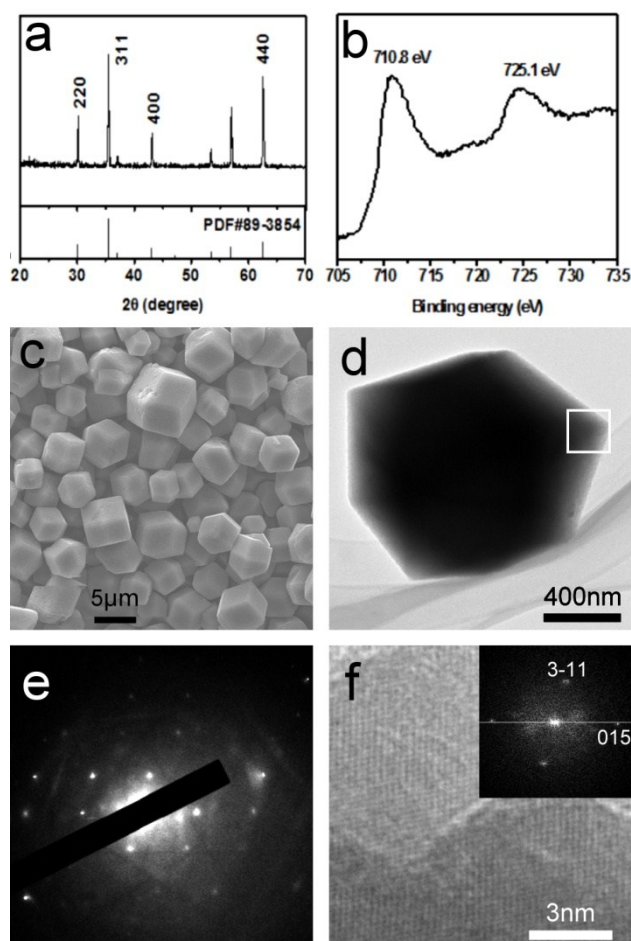
Figure 1. pXRD (a), Fe 2p XPS (b), SEM image (c), TEM (d), SAED pattern from the white square in figure1d (e), HRTEM and FFT (f) of the as-obtained sample 1# of Fe_3O_4 crystals.

Further, other experiments were operated to study the size tune and shape evolution of Fe_3O_4 crystals by controlling some facile experimental conditions. Herein, the effect of α-Fe_2O_3 precursor was firstly studied. Interestingly, the sizes of Fe_3O_4 decahedrons reduce to about 2.5 μm when α-Fe_2O_3 nanoplates (See ESI†, figure S1b) are chosen as precursor (figure 2a). As our previous report and the following discussion, the side surface edges α-Fe_2O_3 nanoplates gradually redissolve and "a mass transport" takes place to change into nanoparticles, which show the α-Fe_2O_3 nanoplates easier to redissolve during solvothermal process than its nanoparticles. Herein, we speculate that the fast growth rate results in the formation of the small sizes of Fe_3O_4 decahedrons because the quick redissolving rates of the platy α-Fe_2O_3 could fast the growth rates of Fe_3O_4 polyhedrons. So the sizes of Fe_3O_4 polyhedrons can be controlled by very facile method in this route. The shape of Fe_3O_4 polyhedrons can change from decahedron into octahedron if the aging temperature low to 180 ℃ (figure 2b). As we all know, Fe_3O_4 octahedrons surrounded by eight {111} facets, and dodecahedral crystals are exposing the {110} basal surfaces.[13] The growth rate of crystals will slow when the reaction temperature decrease from 220 ℃ to 180 ℃, which favours the forming of low-energy octahedron morphology. Specially, the surface smoothness of Fe_3O_4 polyhedrons is different if the aging happen at the different concentration of $N_2H_4 \cdot H_2O$. The surfaces of Fe_3O_4 decahedrons are rough (figure 2c) at the high concentration of $N_2H_4 \cdot H_2O$, and their surfaces are smooth and the edge profiles are clear (figure 2d) at the low concentration of $N_2H_4 \cdot H_2O$ as the reaction medium. The experimental results show that, even in the absence of any surfactants and other additives, the shapes, sizes, and surface characteristics of Fe_3O_4 polyhedrons can facilely control through adopting the route designed in this paper.
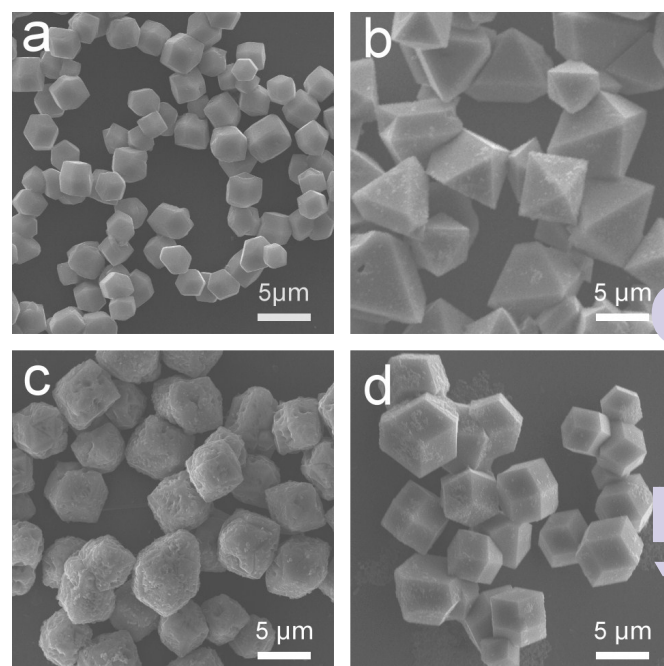
Figure 2. SEM images of the Fe_3O_4 polyhedrons obtained in different condition, (a) sample 2#, (b) sample 3#, (c) sample 4#, (d) sample 5#.

To find out growth mechanism on this interesting evolution route, Herein, the growth process of this route was continuously monitored through collecting the samples from the different curing times, and the phase and morphology were characterized by pXRD，SEM and TEM (figure 3, figure 4).

At reaction times of 1 h, the X-ray diffraction patterns of as-obtained powders are similar to that of α-Fe_2O_3 precursor, and all peaks indexed to a rhombohedral α-Fe_2O_3 (PDF#No.33-0664) without any Fe_3O_4 peaks (figure 3). At reaction times of 2 h, pXRD peaks almost be indexed to the cubic phase of Fe_3O_4, and only weak diffraction peaks of α-Fe_2O_3 can be indexed (marked as "*"), which shows cubic phase of Fe_3O_4 have grown at this time. Prolong the reaction times to 6 h, the diffraction peaks of the cubic Fe_3O_4 are very strong and all of the diffraction peaks indexed α-Fe_2O_3 cannot be identified in figure 3. This indicates there is no α-Fe_2O_3 nanoparticle in the collected sample, or their contents are too low to be detected by XRD method, also maybe some exist as amorphous phase.
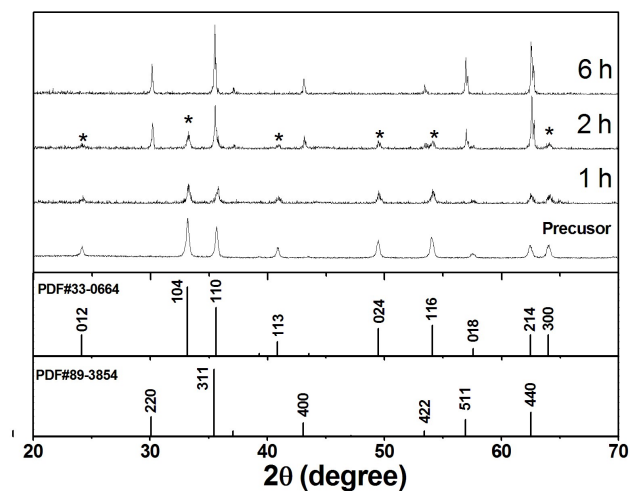
Figure 3. pXRDs of samples obtained at different aging time, the bars are from JCPDS Card No. 89-3854 for spinel structured Fe_3O_4, and No. 33-0664 for α-Fe_2O_3 diffraction peaks.

Seen from SEM and TEM (inset) image in Figure 4a, 4b, the structures of the particles after aging 1 h almost have no difference with α-Fe_2O_3 precursors (Figure S2a), but some micrometer size of products begin to appear, which should be the as-synthesized Fe_3O_4 particles. Some nanoparticles become smaller and the microparticles turn into regular polyhedrons when the reaction times prolong to 2 h (figure 4c, 4d). Prolong the reaction times to 6 h, it is difficult to find out the nanoparticles in the low magnification SEM images (figure 4f), although some nanoparticles can still be "fortunately" found in a certain place in high-magnification SEM image, and their sizes almost reduce to less 10 nm. The TEM image further identifies that the sample is composed from some little nanocrystals (figure 4e (inset)). To further clarify the shapes and structures of the products, HRTEM and FFT are implemented and the results are shown in figure 4g, 4h. The diffraction pattern of the small nanoparticle is indexed as α-Fe_2O_3. According to these experiment results that α-Fe_2O_3 precursors gradually get small and till completely disappear, herein, we can speculate that the

graduate dissolving process of α-Fe_2O_3 precursors should exist in the synthesizing route of Fe_3O_4 polyhedrons.
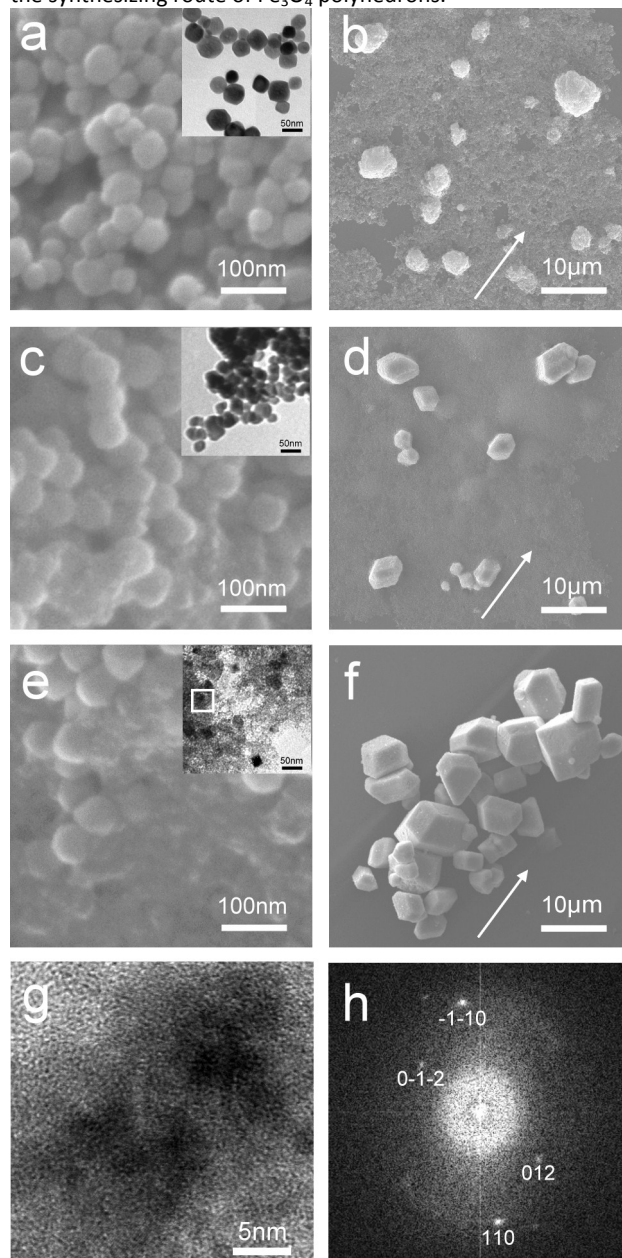
Figure 4. The structures of samples obtained at different aging times, high-magnification SEM image and TEM (inset) (a) 1 h, (c) 2 h, (e) 6 h, low-magnification SEM image, (b) 1 h, (d) 2 h, (f) 6 h, HRTEM (g) from the zone of white square in figure 4e and FFT (h).

The dissolving process of α-Fe_2O_3 precursors can also be further demonstrated according to our previous experimental phenomenon.[19] Therein, the as-synthesized nanoplates (Figure 5a) was added to 10 mL of distilled water. After aging at 180 ℃ for 7 days, the resultant nanocrystals appear with quite different final shapes (Figure 5b). The edges of the nanoplates after aging tend to be round, the nanoplates themselves tend to be thicker, and the diameters tend to be smaller (Figure 5b). We proposed that there is a mass transport from side surfaces to basal surfaces. That is, the side surfaces gradually dissolved and the mass was gradually transported to the basal top (or bottom) (0001) surfaces during the aging stage in water. The results also support our statement about

dissolving phenomenon of α-Fe_2O_3 precursors.
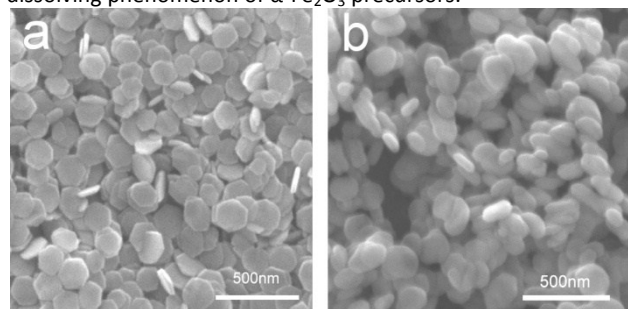
Figure 5. SEM image of α-Fe_2O_3 nanoplates, before aging (a), and

after aging (b) at 180 ℃ for 7 days in the water

So, in this paper, it can be speculated that partly Fe (III) from the dissolving of α-Fe_2O_3 nanoparticles is reduced by $N_2H_4 \cdot H_2O$ into Fe (II) during "a mass transformation", then recrystalize into cubic Fe_3O_4 particles. Xu etc. fabricated 50-facet Fe_3O_4 polyhedron through $FeCl_3 \cdot 6H_2O$ as precursor, and they speculated the formation of Fe_3O_4 particles through the reduction of the possible intermediate phase of $Fe_2O_3 \cdot H_2O$, nucleation of the Fe_3O_4 nuclei and oriented aggregation of the primary nanocrystals.[8] Our experimental phenomena clearly confirm the transformation ways as "dissolving of α-Fe_2O_3 phase-reduction-recrystallization" process. In this route, the growth of crystal is much slower than traditional precipitation methods, so it is favorable to form regular polyhedral shapes. From a crystallographic viewpoint, Fe_3O_4 has a cubic inverse spinel structure with oxygen anions forming a face-centered-cubic (FCC) close-packed structure. As a FCC crystal, a general sequence of surface energies may hold, γ {111} < γ {100} < γ {110}, which indicates that the Fe_3O_4 crystals usually exist with {111} lattice planes as the basal surfaces. So the regular octahedron surrounded by eight {111} facets is easy to be obtained through this route. Usually, some high-energy polyhedron morphology can be obtained under some severe conditions. In this paper, the strong and high concentration reducing agent, along with high temperature can provide a severe reducing environment, which result in the existing of high-energy Fe_3O_4 decahedrons.

Finaly, the magnetic properties of iron oxide nanocrystals were conducted at 300 K. Figure 6a, 6b shows the hysteresis loops of the samples of α-Fe_2O_3 nanoplates and nanoparticles. The weak ferromagnetic behaves and the effects of shape anisotropy on magnetic property have been discussed in our precious paper.[21]

Figure 6c, 6d shows the magnetic hysteresis loop of Fe_3O_4 decahedrons (Samples 1#) and octahedrons (Samples 3#) at 300 K. It can be found that both of the samples are ferromagnetic despite small coercivities (Hc) and remanent fields (Mr). The saturation magnetization (Ms), remanent magnetization (Mr), and coercivity (Hc) of the as-prepared Fe_3O_4 decahedrons are 95.6 emu/g, 9.63 emu/g and 86.9 Oe, respectively. Accordingly, the three values of Fe_3O_4 octahedrons are 102.2 emu/g, 2.17 emu/g and 14.3 Oe, respectively. The low coercivities imply that the as-synthesized Fe_3O_4 nanoparticles are soft magnets. Interestingly, the saturation magnetization of both samples are higher than that (84.5 emu/g) of commercial magnetite fine powder[22] and those reported Fe_3O_4 micro-octahedrons.[12] The great increase suggests the as-grown Fe_3O_4 nanocrystals possess high magnetic moment, which should benefit from the increase of magnetic moment as a result of the noncollinear spin structure originated from the pinning of the surface spins and the clean surface. The values of Hc and Mr increase from 14.3 to 86.9 Oe, and from 2.17 to 9.63 emu/g respectively as the particle shapes change from decahedrons to

octahedrons, which might be as the result of their stronger magnetic anisotropy. The magnetic properties of materials are influenced by many factors, not only size, also crystallinity, surface structure, and so on. However, the higher saturation magnetizations for these two samples make this route deserve to further study and explore their possible industrial applications.
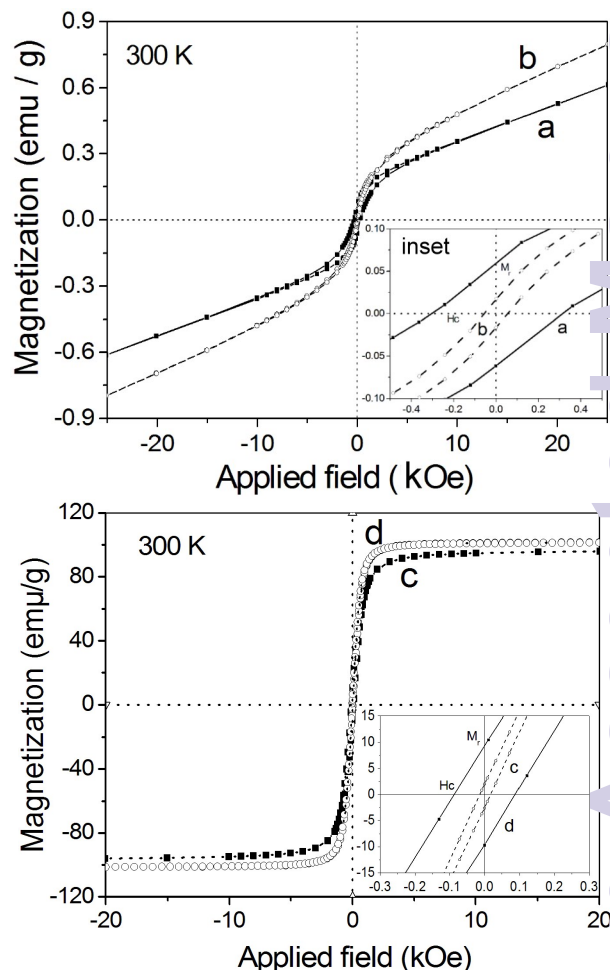
Figure 6. Magnetization-hysteresis (M-H) loops of α-Fe_2O_3 precursors (a) nanoplates, (b) nanoparticles, and as-prepared Fe_3O_4 samples (c) Samples 1#, (d) Samples 3#. The inset is the enlarged ones in the range of -0.3 and 0.3 KOe.

In conclusion, we adopted α-Fe_2O_3 as precursor to realize the growth of Fe_3O_4 polyhedrons. The transformation process from α-Fe_2O_3 to cubic Fe_3O_4 is confirmed through "dissolution-reduction-recrystallization". The reaction system in this method is simple and the as-obtained samples are dispersed with a clean surface due to only the addition of hydrazine hydrate, without any other surfactants or reagents. This route not only provides the convenience for the research of growth mechanism, also provides a practical method to controllably prepare high quality iron oxides and some other iron-based compounds. Fe_3O_4 polyhedrons obtained through this route show very high saturation magnetization.

Notes and references

1 H. G. Cha, C. W. Kim, S. W. Kang, B. K. Kim and Y. S. Kang, *J. Phys. Chem. C.*, 2010, **114**, 9802.
2 (a) Y. Du, W. Liu, R. Qiang, Y. Wang, X. Han, J. Ma and P. Xu, *ACS Appl. Mater. Inter.,* 2014, **6**, 12997; (b) G. Sun, B. Dong, M. Cao, B. Wei and C. Hu, *Chem. Mater.*, 2011, **23**, 1587.
3 W. P. Li, P. Y. Liao, C. H. Su and C. S. Yeh, *J. Am. Chem. Soc.*, 2014, **136**, 10062.
4 Z. Zhou, Z. Zhao, H. Zhang, Z. Wang, X. Chen, R. Wang, Z. Chen and J. Gao, *ACS nano.*, 2014, **8**, 7976.
5 K. Cheng, S. Peng, C. Xu and S. Sun, *J. Am. Chem. Soc.*, 2009, **131**, 10637.
6 X. L. Cheng, J. S. Jiang, D. M. Jiang and Z. J. Zhao, *J. Phys. Chem. C.*, 2014, **118**, 12588.
7 (a) Q. An, F. Lv, Q. Liu, C. Han, K. Zhao, J. Sheng, Q. Wei, M. Yan and L. Mai, *Nano Lett.*, 2014, **14**, 6250; (b) D. Chen, G. Ji, Y. Ma, J. Y. Lee and J. Lu, *ACS Appl. Mater. Inter.*, 2011, **3**, 3078; (c) J. Zhao, B. Yang, Z. Zheng, J. Yang, Z. Yang, P. Zhang, W. Ren and X. Yan, *ACS Appl. Mater. Inter.*, 2014, **6**, 9890.
8 Y. Xu, H. Hao, P. Liu, Q. Wang, Y. Sun and G. Zhang, *CrystEngComm*, 2014, **16**, 10451.
9 (a) M. Song, Y. Zhang, S. Hu, L. Song, J. Dong, Z. Chen and N. Gu, *Colloid Surf. A-Physicochem. Eng. Asp.*, 2012, **408**, 114; (b) Z. Cheng, X. Chu, J. Yin, H. Zhong and J. Xu, *Mater. Lett.*, 2012, **75**, 172.
10 (a) M. A. Daniele, M. L. Shaughnessy, R. Roeder, A. Childress, Y. P. Bandera and S. Foulger, *ACS nano*, 2012, **7**, 203; (b) S. Kohiki, T. Kinoshita, K. Nara, K. Akiyama-Hasegawa and M. Mitome, ACS *Appl. Mat. Inter.*, 2013, **5**, 11584; (c) X. Qi, N. Li, Q. Xu, D. Chen, H. Li and J. Lu, *RSC Adv.*, 2014, **4**, 47643.
11 C. H. Hsia, T. Y. Chen and D. H. Son, *J. Am. Chem. Soc.*, 2009, **131**, 9146.
12 (a) J. Sato, M. Kobayashi, H. Kato, T. Miyazaki and M. Kakihana, *J. Asian. Ceram. Soc.*, 2014, **2**, 258; (b) Z. Chen, Z. Geng, T. Tao and Z. Wang, *Mater, Lett.*, 2014, **117**, 10; (c) D. E. Zhang, X. J. Zhang, X. M. Ni, J. M. Song and H. G. Zheng, *Cryst. Growth. Des.*, 2007, **7**, 2117.
13 B. Y. Geng, J. Z. Ma and J. H. You, *Cryst. Growth. Des.*, 2008, **8**, 1443.
14 S. Ayyappan, G. Gnanaprakash, G. Panneerselvam, M. P. Antony and J. Philip, *J. Phys. Chem. C.*, 2008, **112**, 18376.
15 M. H. Rashid, M. Raula and T. K. Mandal, *Mater.Chem. Phys.,* 2014, **145**, 491.
16 H. T. Hai, H. Kura, M. Takahashi and T. Ogawa, *J.* Colloid Interface *Sci.*, 2010, **341**, 194.
17 S. H. Xuan, L. Y. Hao, W. Q. Jiang, L. Song, Y. Hu, Z. Y. Chen, L. F. Fei and T. W. Li, *Cryst. Growth. Des.*, 2007, **7**, 430.
18 C. H. Ho, C. P. Tsai, C. C. Chung, C. Y. Tsai, F. R. Chen, H. J. Lin and C. H. Lai, *Chem. Mater.*, 2011, **23**, 1753.
19 L. Chen, X. Yang, J. Chen, J. Liu, H. Wu, H. Zhan, C. Liang and M. Wu, *Inorg. Chem.*, 2010, **49**, 8411.
20 J. Lu, X. Jiao, D. Chen and W. Li, *J. Phys. Chem. C.,* 2009, **113**, 4012.
21 L. Chen, W. Liu, J. Chen, X. Yang, J. Liu, H.Fu, M. Wu, *Sci China Chem.,* 2011, **54**, 923.
22 (a) H. Zhou, R. Yi, J. Li, Y. Su, X. Liu, *Solid State Sci.*, 2010, 12, 99. (b) P. Guardia, B. Batlle-Brugal, A. Roca, O. Iglesias, M. Morales, C. Serna, A. Labarta and X. Batlle, *J. Magn. Magn. Mater.*, 2007 **316**, e756.